PCCP

Accepted Manuscript

ROYAL SOCIETY OF CHEMISTRY

www.rsc.org/pccp

Effects of oxygen impurity and nitrogen vacancy on surface properties of the Ta_3N_5 photocatalyst: a DFT study

Jiajia Wang,[ab] Aibin Ma,[*ac] Zhaosheng Li,[*b] Jinghua Jiang,[ac] Jianyong Feng[b] and Zhigang Zou[b]

[a] *College of Mechanics and Materials, Hohai University, Nanjing 210098, China.*

[b] *National Laboratory of Solid State Microstructures, Department of Physics, Ecomaterials and Renewable Energy Research Center (ERERC), and College of Engineering and Applied Sciences, Nanjing University, Nanjing 210093, People's Republic of China.*

[c] *Jiangsu collaborative innovation center of advanced micro/nano materials & equipment, Nanjing 210094, China.*

* Corresponding Authors: Tel: +86-25-83787239, Fax: +86-25-83786046.

E-mail:aibin-ma@hhu.edu.cn(A.B. MA) or zsli@nju.edu.cn(Z. S. Li)

Abstract: Surface defects and impurities play important roles in the photocatalytic performance of semiconductors. In this study, the DFT calculations are performed to investigate effects of oxygen impurity and nitrogen vacancy on surface stabilities and electronic structures of Ta_3N_5 (100), (010) and (001) low-index surfaces. The results show that, for each surface, the oxygen impurity and nitrogen vacancy are beneficial and harmful, respectively, to surface stabilities of Ta_3N_5. The oxygen impurity and nitrogen vacancy mainly have two effects on the surface electronic structures of Ta_3N_5. One is saturating surface states on the clean surface; the other is inducing the downshift of conduction band minimum. In addition, the Ta_3N_5 (100) surface with oxygen impurity is expected to have the strongest reduction ability in practice, providing useful guidance for further investigations of Ta_3N_5 in the photocatalytic hydrogen evolution.

1. Introduction

Semiconductor-based photocatalytic or photoelectrochemical (PEC) water splitting is a promising strategy for solving energy shortage and environmental crisis, because it supplies an environmentally approach to split water into H_2 and O_2 under irradiation of solar light. Since the pioneer work by Fujishima and Honda,[1] metal oxides such as $BiVO_4$,[2] Fe_2O_3[3] and WO_3[4] have been extensively studied. However, due to the large band gaps or insufficient redox potentials, the photocatalytic activities of most metal oxides are not high. Recently, the tantalum nitride (Ta_3N_5) emerges as one promising candidate for photocatalytic or PEC water splitting.[5-10] Due to the smaller band gap (about 2.1 eV), Ta_3N_5 is able to absorb more visible portion of the solar light. Moreover, the valence band maximum (VBM) and conduction band minimum (CBM) of Ta_3N_5 straddle the water oxidization (H_2O/O_2) and reduction (H^+/H_2) potentials, suggesting that Ta_3N_5 theoretically has sufficient redox potentials to split water into H_2 and O_2.

Although Ta_3N_5 is theoretically an ideal photocatalyst, its practical photocatalytic and PEC performances are unsatisfactory. In recent years, great efforts such as loading of cocatalysts,[11, 12] morphology control[13-16] and elements doping[17-21] have been made to improve the photocatalytic and PEC activities of Ta_3N_5. Unfortunately, the current solar-to-hydrogen (STH) efficiency of Ta_3N_5 is merely 1.5%,[19] which is much smaller than its maximum theoretical STH efficiency of 15.9%[22] (under AM 1.5 G irradiation).

One proper cause of the lower practical photocatalytic activities of Ta_3N_5 comes from the inner defects or impurities. In Ta_3N_5, the nitrogen vacancy (V_N) is the major intrinsic defect because anion vacancies such as nitrogen vacancy and oxygen vacancy

are usually the most common defects in metal nitrides and oxides, respectively. Besides the V_N, the practical Ta_3N_5 naturally consists of abundant oxygen impurities which exist in the form of substitution for nitrogen (O_N).[23, 24] One proper source of the O_N impurities is the residual O of Ta_2O_5 precursor after the nitridation treatment. Furthermore, the O_N impurities are very difficult to be totally eliminated under different growth conditions.[24] Our theoretical calculations reveal that the O_N impurities help maintain the mechanical stability and strengthen the atomic cohesion within Ta_3N_5,[25] validating that the natural existence of O_N impurity is theoretically favorable in Ta_3N_5.

Generally, defects and impurities affect photocatalytic performance of semiconductors by regulating some important properties such as band gaps, band edge positions and surface properties. To our knowledge, effects of O_N and V_N on band gap and band edge positions of Ta_3N_5 have been extensively studied from experiments[23, 24] and theoretical calculations,[26-28] while that on surface properties of Ta_3N_5 are still less known. Based on the density functional theory (DFT) calculations, the surface energies and electronic structures of Ta_3N_5 (100) surface with O_N and V_N have been studied by our previous work.[29] However, besides the (100) surface, other typical low-index surfaces such as the (010) and (001) surfaces are also important for Ta_3N_5, thus the effects of O_N and V_N on these low-index surfaces should be studied either. Although Watanabe *et al.*[30] compared the (100), (010) and (001) surfaces of Ta_3N_5 by DFT calculations, effects of O_N and V_N on (010) and (001) surfaces were still not investigated in their work.

The motivation of this study is to make an in-depth understanding of surface

properties of Ta_3N_5 with O_N and V_N. Experimental study of semiconductor surfaces is sometimes a challenging task, while theoretical investigations, for example the DFT calculations, are easily able to provide microscopic descriptions of surface properties. To our knowledge, the most stable surface of Ta_3N_5 has not been experimentally investigated. Considering that the Ta_3N_5 semiconductor is orthorhombic lattice, we choose the typical (100), (010) and (001) low-index surfaces to perform surface property investigations for Ta_3N_5. Based on the DFT calculations, effects of O_N and V_N on surface stabilities and electronic structures of Ta_3N_5 (100), (010) and (001) surfaces will be investigated in this study. Our calculations will not only elucidate experimental observations associated with Ta_3N_5, but also provide useful guidance for improving photocatalytic activities of Ta_3N_5.

2. Computational details

2.1 Computational method

The DFT calculations in this study are performed by the VASP[31, 32] with the projected-augmented-wave (PAW[33]) method. All the DFT calculations are performed in the unrestricted formalism. For the exchange-correlation functional, the generalized gradient approximation (GGA[34]) in the scheme of Perdew-Bueke-Ernzerhof (PBE[35]) is used. For N, O and Ta, the $2s^2 2p^3$, $2s^2 2p^4$ and $5p^6 5d^4 6s^1$ orbital, respectively, are treated as valence states. The cutoff energy for basis functional is 500 eV. Geometry relaxations are performed until the residual forces on each ion converged to be smaller than 0.02 eV $Å^{-1}$.

It is worthy of mentioning that, due to underestimation of band gap, the PBE functional is sometimes not accurate enough to calculate electronic structures of semiconductors. Using the hybrid functional, for example the Heyd-Scuseria-Ernzerhof (HSE[36]) functional, is able to get more accurate results, but the computational cost of HSE is much more than that of PBE. In our previous work, the PBE and HSE functional were both adopted to calculate electronic structures of the bulk Ta_3N_5 with O_N and V_N.[25] The results showed that the in-gap defect states and band edge shift calculated by PBE were in good agreement with that by HSE, suggesting that the PBE functional was sufficient to make reasonable qualitative analysis for Ta_3N_5.

2.2 Surface energy calculation method

Surface energies of Ta_3N_5 surfaces with and without defects are calculated using the following equation[37]:

$$E_{\text{surf}} = [E_{slab} - \sum_i n_i(\Delta\mu_i + E_i)]/(2A) \quad (1)$$

where E_{slab} is the total energy of the slab model, n_i and $\Delta\mu_i$ (i=N, O, Ta) are the number and chemical potential of constituent i, respectively, and E_i (i=N, O, Ta) is the energy per atom in the source element. The chemical potential calculation details can be found in SI-1 of the electronic support information (ESI). A is the surface area of the slab model. If the factor '2' is not divided in Eqn. (1), the calculated surface energies are the sum of top and bottom ends of the slab model. Since the top and bottom ends of the constructed slab model are identical, the factor '2' should be divided. More surface energy calculation details can be found in SI-2 of the ESI.

2.3 Surface models

To simulate different Ta_3N_5 surfaces, we firstly perform geometry relaxation of the conventional bulk Ta_3N_5, whose atomic structure is shown in Fig. 1a. The relaxed lattice constants of the conventional bulk Ta_3N_5 are a=3.91, b=10.32 and c=10.35 Å, which agree within the estimated experimental uncertainty (a=3.89, b=10.21 and c=10.26 Å).[38] Then, the (100), (010) and (001) surfaces are constructed by cutting through corresponding planes of the conventional bulk Ta_3N_5.

Fig. 1b to d show the slab models of Ta_3N_5 (100), (010) and (001) surfaces, respectively. It is seen that: (i) The Ta_3N_5 (100) surface is very simple because it has only one termination. (ii) The Ta_3N_5 (010) surface is a little complex because it may be exposed by different terminations. Since it is difficult to enumerate all terminations of the (010) surface, we consider three possible terminations which are named as T1, T2, and T3, respectively. During the geometry relaxation, however, the two outmost N atoms on the T1 termination leave away from the surface, and the T1 termination finally becomes the T2 termination. Therefore, only T2 and T3 terminations are finally considered for the (010) surface. (iii) Similar with the (010) surface, the (001) surface is also complex and three terminations T1, T2 and T3 are considered for the (001) surface. In this study, the top and bottom ends of each constructed slab model are identical, thus the dipole correction[39] is not needed. More discussion of different surface terminations can be found in SI-3 of the ESI.

As can be seen in Fig. 1a, the Ta atom is coordinated with six neighboring N atoms,

while N atoms are coordinated with three (N3) or four (N4) Ta atoms. Then, the N3 and N4 sites should be both considered to construct oxygen impurity and nitrogen vacancy. For clarity purpose, all considered terminations in this study are denoted by the combination of surface name, termination name and defect name. For example, the T2 termination of (001) surface with and without the V_{N3} are denoted by $(001)_{T2}$+V_{N3} and $(001)_{T2}$, respectively. Since only one termination is considered for the (100) surface, the termination name is not needed for describing the (100) surface. For example, the (100) surface with and without the O_{N3} can be easily denoted by (100)+O_{N3} and (100), respectively. What should be noted is that, when the (010) surface is terminated with the T2 and T3 terminations, the N atoms are mainly exposed by the N3 and N4 atoms, respectively. Therefore, the N3 atom is adopted to construct O_N and V_N for $(010)_{T2}$, while the N4 atom is adopted to construct O_N and V_N for $(010)_{T3}$.

To ensure the reliability of calculated surface properties, all slab models should be constructed by sufficient number of atomic layers. The convergence of atomic layers for different surfaces has been carefully tested by calculating surface energies. More details of the convergence test, as well as other important computational parameters, can be found in SI-4 of the ESI.

3. Results and discussion

3.1 The properties of bulk Ta_3N_5

Although the properties of bulk Ta_3N_5 have been extensively studied in other theoretical work,[40, 41] it is still necessary to make a discussion of the bulk Ta_3N_5 before discussing

the surface properties. Fig. 2a and b show band structures calculated by the primitive cell and conventional cell, respectively, of the pure bulk Ta_3N_5. Due to the band gap underestimation of the PBE functional, the calculated band gap of Ta_3N_5 is smaller than the experimental band gap (about 2.1 eV). Fig. 2a reveals that Ta_3N_5 is an indirect gap semiconductor, with VBM and CBM locating at the Γ and Y points, respectively. The indirect (Γ-Y) and direct (Γ-Γ) band gaps are 1.27 and 1.50 eV, respectively, which agree well with other theoretical work.[41] The band gap in Fig. 2b calculated by the conventional cell is still 1.27 eV. However, due to the Brillouin zone (BZ) folding effects, the VBM and CBM in Fig. 2b are both locating at the Γ point, resulting in the direct gap character of Ta_3N_5.

In this study, to investigate the surface electronic structures, the projected band structures of clean Ta_3N_5 surfaces will be calculated in below Section 3.3. We originally used the conventional cell of bulk Ta_3N_5 to calculate the projected band structures, because the conventional cell of Ta_3N_5 was orthorhombic lattice, which was very convenient for constructing the (100), (010) and (001) surfaces. Unfortunately, due to the BZ folding effects, the conventional cell was not suitable for calculating the projected band structures. Therefore, in below Section 3.3, the projected band structures are calculated by using the primitive cell of bulk Ta_3N_5. More details of the projected band structure calculation can be found in SI-5 of the ESI.

Effects of O_N and V_N on electronic structures of the bulk Ta_3N_5 have been studied elsewhere.[27, 42] Fig. 3 shows the schematic band structures (data derive from Ref. 42) of the bulk Ta_3N_5 with O_N (Ta_3N_5+O_N) and V_N (Ta_3N_5+V_N). In Ta_3N_5, the O_N and V_N are

both electron donors. Due to the extremely low defect transition energy for reducing Ta atoms in Ta_3N_5,[42] the donated electrons from O_N and V_N are easily able to reduce the Ta atoms, which further induce the downshift of CBM of the bulk Ta_3N_5. For the V_N which donates more electrons than O_N, besides the electrons that reduce the Ta atoms, the rest of electrons induce an in-gap defect state whose charge densities are mainly localized near the V_N site. Although the O_N and V_N are both electron donors, their effects on the structural stability of Ta_3N_5 are totally different.[25] The O_N impurity strengthens the atomic cohesion within the Ta_3N_5 thus improving the structural stability, while the V_N defect is harmful to the structural stability of Ta_3N_5.

3.2 Surface stabilities

In this section, we begin to discuss surface stabilities of Ta_3N_5. Surface stabilities can be thermodynamically evaluated by surface energies. Generally, the smaller the surface energy is, the more stable the surface will be. Fig. 4a to f show surface energies of (100), $(010)_{T2}$, $(010)_{T3}$, $(001)_{T1}$, $(001)_{T2}$ and $(001)_{T3}$, respectively, with and without O_N and V_N as a function of the chemical potential of N ($\Delta\mu_N$). The negative and zero $\Delta\mu_N$ correspond to the N-poor and N-rich growth conditions, respectively. The Ta_3N_5 semiconductor is usually prepared by the nitridation treatment of the Ta_2O_5 precursor, thus more attentions should be paid to the N-rich growth condition.

The surface energies of (100), (010) and (001) surfaces have two common grounds. First, regardless of the growth conditions, the surface energies of (100), (010) and (001) surfaces with O_{N3} and V_{N3} are smaller than that with O_{N4} and V_{N4}, respectively. This is

consistent with the experimental observation that the O atom mainly substitutes the N3 atom but not the N4 atom.[24] Then, calculation and discussion hereinafter only consider O_{N3} and V_{N3}. Second, under the N-rich growth condition, the surface energies of (100), (010) and (001) surfaces with V_N are always the largest, suggesting that the V_N defect is harmful to surface stability of Ta_3N_5. This is consistent with previous theoretical work that the V_N defect is harmful to structural stability of the bulk Ta_3N_5.[25]

As mentioned above, the O_N impurity naturally exists in Ta_3N_5. Previous theoretical work provides two proper explanations to this phenomenon. One is that the O_N impurity is beneficial to structural stability of Ta_3N_5 by improving the mechanical stability,[25] the other is that the O_N impurity helps stabilize the Ta_3N_5 (100) surface by decreasing surface energy of the clean (100) surface.[29] In this study, besides the (100) surface (Fig. 4a), we find that surface energies of $(010)_{T2}$+O_{N3} (Fig. 4b) and $(001)_{T2}$+O_{N3} (Fig. 4e) are also smaller than that of clean $(010)_{T2}$ and $(001)_{T2}$ surfaces, respectively. This result further confirms that the O_N impurity is beneficial to surface stability of Ta_3N_5, providing stronger explanations to the natural existence of O_N impurity in Ta_3N_5.

Note that, when the (010) surface is terminated with the T3 termination (Fig. 4c), the surface energy of clean $(010)_{T3}$ is smaller than that of $(010)_{T3}$+O_{N4} under the N-rich growth condition, suggesting that the O_N impurity does not always play a positive role in stabilizing Ta_3N_5 surfaces. However, for the (010) surface, regardless of whether the surface is clean or not, the surface energies of T3 termination are much bigger than that of T2 termination (Fig. 4b). Although it is inappropriate to determine the exact

termination of a surface merely by comparing surface energies, termination with smaller surface energy is generally more stable and has more possibilities to be exposed.[43] Therefore, due to the smaller surface energies, the T2 termination is expected to occupy the major part of the (010) surface. Similar conclusions can also be arrived at the (001) surface, whose major termination should be the T2 termination either. Then, for the simplicity purpose, only the T2 termination is considered for both the (010) and (001) surfaces in the following electronic structure calculations.

3.3 Surface electronic structures

Fig. 5a-c, d-f and g-i show density of states (DOS) of the (100), $(010)_{T2}$ and $(001)_{T2}$ surfaces, respectively, with and without O_{N3} and V_{N3}. The DOS in Fig. 5a-c (the same for d-f and g-i) correspond to (100), (100)+O_{N3} and (100)+V_{N3} surfaces, respectively. It is seen that:

(i) In Fig. 5a, the band gap of (100) surface is about 0.8 eV, which is much smaller than that of the bulk Ta_3N_5 (1.27 eV). Such a smaller band gap of (100) is properly coming from the surface states on the clean (100) surface, because the 0.8 eV band gap may be ascribed to the energy separation between surface states and CBM. However, no obvious evidences can be seen for the presence of surface states in Fig. 5a. What should be mentioned is that, in our previous DFT investigation on the clean Ta_3N_5 (100) surface,[29] one surface state is clearly observed on the top of VBM because the surface state lies alone in the band gap. In this study, when a denser *k*-point mesh (12×12×12) is used, we find that the surface state is not alone in the band gap but mixed with the VBM,

leading to the difficulty in recognizing surface states in Fig. 5a (more details of the effects of *k*-points on the DOS of Ta_3N_5 (100) surface can be found in SI-6 of the ESI). To reveal the truth of surface states on Ta_3N_5 (100) surface, the band structure of the clean (100) surface, together with its projected band structure (shaded area), are shown in Fig. 6a. It is seen that, two surface states B1 and B2 lie on the top of VBM, suggesting that the 0.8 eV band gap of the clean (100) surface in DOS results is indeed coming from the energy separation between surface states and CBM. Partial charge densities of B1 and B2 states are mainly distributed on the N atoms of top atomic layers, further confirming that the B1 and B2 states are both surface states on Ta_3N_5 (100) surface.

In Fig. 5b and c, in which the O_{N3} and V_{N3}, respectively, are introduced onto the clean (100) surface, the CBM of (100)+O_{N3} and (100)+V_{N3} shift left compared with that of the clean (100) surface. Furthermore, the energy separations between VBM and CBM of (100)+O_{N3} and (100)+V_{N3} gradually increase compared with that of the clean (100) surface. We also calculate surface band structures of (100)+O_{N3} and (100)+V_{N3}, which are shown in Fig. 6b and c, respectively. Partial charge densities of the downshift B3 and B5 states are both uniformly distributed on all Ta atoms. This is consistent with the discussion in Fig. 3 that the O_N and V_N are both able to reduce Ta atoms, which further induces the downshift of CBM of the bulk Ta_3N_5. Besides the downshift of CBM, another important effect induced by O_N and V_N is the saturation of surface states. Compared with the clean (100) surface, the (100)+O_{N3} has only one B4 surface state on the top of VBM. In (100)+V_{N3}, the surface states completely disappear.

(ii) Fig. 5d-f show DOS of $(010)_{T2}$, $(010)_{T2}$+O_{N3} and $(010)_{T2}$+V_{N3}, respectively. Similar with the clean (100) surface, the clean $(010)_{T2}$ surface also has a smaller band gap. The surface and projected band structures of the clean $(010)_{T2}$ surface in Fig. 7a show that two surface states B1 and B2 locate on the top of VBM, leading to the smaller band gap of the clean $(010)_{T2}$ surface. The effects of O_N and V_N on electronic structures of clean $(010)_{T2}$ surface are also similar with that of the clean (100) surface. First, the O_N and V_N are both able to saturate surface states on the clean $(010)_{T2}$ surface. Second, the O_N and V_N are both able to reduce the Ta atoms (see B3 and B5 states), which further induce the downshift of CBM.

What the major difference between the $(010)_{T2}$ and (100) surfaces is that, the O_N and V_N are both able to induce in-gap defect states (B4 in Fig. 7b and B6 in Fig. 7c), which are not seen in (100)+O_{N3} and (100)+V_{N3}. Partial charge densities reveal that the electrons of B4 and B6 states are mainly localized in the spaces next to O_{N3} and V_{N3}, respectively. The B6 state in the band gap of $(010)_{T2}$+V_{N3} is theoretically reasonable because similar defect state is also presented in the band gap of bulk Ta_3N_5+V_N (as shown in Fig. 3). What is beyond expectation is that the O_N also induces an in-gap defect state B4. The above surface energies provide proper explanations to the in-gap state of $(010)_{T2}$+O_{N3}. As can be seen in Fig. 4b, under the N-rich growth condition, the surface energy of $(010)_{T2}$+O_{N3} is not obviously smaller but very close to that of the clean $(010)_{T2}$ surface. This means that, unlike the clean (100) and $(001)_{T2}$ surfaces, the clean $(010)_{T2}$ surface does not extremely need the O_N to improve its surface stability. In other words, the donated electrons from O_N are not extremely needed for $(010)_{T2}$,

leading to the in-gap state B4 and its localized charge distribution.

(iii) For $(001)_{T2}$, $(001)_{T2}$+O_{N3} and $(001)_{T2}$+V_{N3}, their DOS results and corresponding surface band structures are shown in Fig. 5g-i and 8a-c, respectively. Cutting the bulk Ta_3N_5 through the $(001)_{T2}$ surface also introduces a surface state (B1 in Fig. 8a), which is consistent with the situations in clean (100) and $(010)_{T2}$. However, unlike the clean (100) and $(010)_{T2}$ surfaces whose surface states are below the Fermi level, the B1 state of clean $(001)_{T2}$ surface locates above the Fermi level, suggesting that the B1 state is not occupied with electrons but with holes. Since the O_N is an electron donor, the charge compensation is expected to considerably facilitate doping of O_N onto the $(001)_{T2}$ surface. This may be the reason why the surface energy of $(001)_{T2}$+O_{N3} largely drops compared with that of the clean $(001)_{T2}$ surface (as shown in Fig. 4e).

In Fig. 8b, based on the charge compensation mechanism, the surface states disappear in the band gap of $(001)_{T2}$+O_{N3}. Furthermore, since the electrons donated from O_{N3} have compensated with the B1 state, no more electrons can reduce the Ta atoms, thus the CBM of $(010)_{T2}$+O_{N3} does not shift down. In Fig. 8c, when the V_{N3} is introduced onto the clean $(001)_{T2}$ surface, the surface state B1 also disappears because of the charge compensation between B1 state and V_{N3}. In addition, since V_{N3} donates more electrons than O_{N3}, the rest of electrons donated from V_{N3} induce the B2 state, whose charge densities are mainly localized in the space next to the V_{N3} site. What should be noted is that, the B2 state is obviously below the CBM in Fig. 8c, while the corresponding states of B2 state in the DOS results (Fig. 5i) almost interact with the CBM. Actually, the surface band structures of Fig. 8a-c are calculated along the Y-Γ and

Γ-S surface BZ paths. For the visualization purpose, only band structure along the Γ-S path is shown in Fig. 8a-c, leading to the disagreement between surface band structures and DOS results. If the Y-Γ and Γ-S paths are both adopted for presentation, the surface band structures will be in good agreement with the DOS results. More details of the surface band structures of Fig. 8c can be found in SI-7 of the ESI. In addition, due to the delocalized character of the GGA functional, the HSE calculations with single Γ point are also performed to verify the GGA results, which can be found in SI-8 of the ESI.

3.4 Discussion

As mentioned above, surfaces with smaller surface energies are thermodynamically more stable and have more possibilities to be exposed.[43] Therefore, due to the smaller surface energies, the (100)+O_{N3}, $(010)_{T2}$+O_{N3} and $(001)_{T2}$+O_{N3} have more possibilities to be exposed for the (100), (010) and (001) surfaces, respectively. Electronic structures reveal that, except the $(001)_{T2}$+O_{N3}, the CBM of (100)+O_{N3} and $(010)_{T2}$+O_{N3} are both occupied with electrons which are uniformly distributed on the Ta atoms. Since the electrons on reduced Ta atoms are very easy to transfer,[42] the reduction abilities of (100)+O_{N3} and $(010)_{T2}$+O_{N3} are expected to be stronger than that of $(001)_{T2}$+O_{N3}.

To confirm the above discussion, we use the Cl atom as a probe to compare the reduction abilities of (100)+O_{N3}, $(010)_{T2}$+O_{N3} and $(001)_{T2}$+O_{N3}. Due to the strong electronegativity of Cl element, the reduction abilities of Ta_3N_5 surfaces can be evaluated by the charge integrated on Cl atoms, which is calculated by the Bader[44] population analysis. The charge integrated on Cl, as well as the adsorption energy of Cl

on (100)+O_{N3}, $(010)_{T2}$+O_{N3} and $(001)_{T2}$+O_{N3} surfaces are listed in Table 1 (More details of the adsorption calculation can be found in SI-9 of the ESI). Since the more electrons integrated on Cl indicate the stronger reduction ability of the surface, the $(010)_{T2}$+O_{N3} surface shows the strongest reduction ability, while the $(001)_{T2}$+O_{N3} shows the lowest reduction ability. This is in good agreement with the above electronic structure analysis. Moreover, the order of charge integrated on Cl is also in good agreement with that of adsorption energies. Therefore, the charge integrated on Cl and the adsorption energies provide reasonable evaluation for the reduction abilities of different Ta3N5 surfaces.

Although the $(010)_{T2}$+O_{N3} theoretically shows the strongest reduction ability, its practical reduction ability may be weakened by the surface terminations. As discussed in Fig. 4b, under the N-rich growth condition which is usually the practical growth condition of Ta_3N_5, the surface energy of $(010)_{T2}$+O_{N3} is very close to that of the $(010)_{T2}$ surface, suggesting that the $(010)_{T2}$ and $(010)_{T2}$+O_{N3} have the same possibilities to be exposed. Since the CBM of $(010)_{T2}$ is not occupied with electrons, the reduction ability of $(010)_{T2}$ is lower than that of $(010)_{T2}$+O_{N3}. When the $(010)_{T2}$ is partly exposed on the (010) surface, the reduction ability of (010) surface will be weakened. Therefore, the practical reduction ability of the (010) surface may be not as high as expectation. In other words, the (100) surface is expected to have stronger reduction ability in practice.

Our calculation results are consistent with Lu *et al.*' experiments.[45] To our knowledge, Lu *et al.* used to synthesize a needle-like Ta_3N_5, which was controlled to grow along the [100] direction. Then, only two ends of the needle-like Ta_3N_5 were (100) plane. Lu *et al.* found that, when the sacrificial $AgNO_3$ was used in the experiment, the

pure Ag metals were only observed to deposit on the (100) surface but not on other surfaces. Since electrons are needed for the transition from Ag^+ ion to Ag metal, this experiment suggests that the Ta_3N_5 (100) surface is more reductive than other surfaces in practice, agreeing with our calculation results. In addition, their experiments revealed that the photocatalytic H_2 evolution abilities of the needle-like Ta_3N_5 were much weaker than that of the common bulk Ta_3N_5, which was also explained by the fewer reductive (100) surfaces of the needle-like Ta_3N_5. Therefore, in further experimental studies on Ta_3N_5, more attentions should be paid to the (100) surface because this surface plays the vital role in the photocatalytic performance of Ta_3N_5.

4. Conclusions

In summary, based on the DFT calculations, the effects of O_N and V_N on surface properties of Ta_3N_5 (100), (010) and (001) surfaces are detailed investigated in this study. For each surface, we find that the O_N impurity is beneficial to surface stability, providing strong explanations to the natural existence of O_N impurity in Ta_3N_5. By calculating surface and projected band structures, we find that there are surface states on the clean (100), (010) and (001) surfaces. When the O_N and V_N are introduced onto the clean surface, the surface states on clean surface are saturated, along with the downshift of CBM or appearance of in-gap defect states. Furthermore, using the single Cl atom as a probe, we compare the reduction abilities of (100), (010) and (001) surfaces. It is found that the (100) surface shows the strongest reduction ability in practice, which is expected to be helpful for further investigations of the Ta_3N_5 photocatalyst.

Acknowledgements

This work is supported by National Basic Research Program of China (973 Program, 2013CB632404), a Project Funded by the Priority Academic Program Development of Jiangsu Higher Education Institutions, New Century Excellent Talents in University (NCET-12-0268), the National Natural Science Foundation of China (No. 51272102), Natural Science Foundation of Jiangsu Province of China (Grant No. BK20131373), National Natural Science Foundation of China (Grant No. 51141002) and China Postdoctoral Science Foundation funded project (Grant No. 2015M570400). We are also grateful to the High Performance Computing Center (HPCC) of Nanjing University for doing the numerical calculations in this paper on its IBM Blade cluster system.

References

1. A. Fujishima and K. Honda, *Nature*, 1972, **238**, 37-38.
2. W. J. Luo, Z. S. Yang, Z. S. Li, J. Y. Zhang, J. G. Liu, Z. Y. Zhao, Z. Q. Wang, S. C. Yan, T. Yu and Z. G. Zou, *Energy Environ. Sci.*, 2011, **4**, 4046-4051.
3. A. Duret and M. Gratzel, *J. Phys. Chem. B*, 2005, **109**, 17184-17191.
4. D. Chen and J. Ye, *Adv. Funct. Mater.*, 2008, **18**, 1922-1928.
5. W. J. Chun, A. Ishikawa, H. Fujisawa, T. Takata, J. N. Kondo, M. Hara, M. Kawai, Y. Matsumoto and K. Domen, *J. Phys. Chem. B*, 2003, **107**, 1798-1803.
6. A. Ishikawa, T. Takata, J. N. Kondo, M. Hara and K. Domen, *J. Phys. Chem. B*, 2004, **108**, 11049-11053.
7. X. J. Feng, T. J. LaTempa, J. I. Basham, G. K. Mor, O. K. Varghese and C. A. Grimes, *Nano Lett.*, 2010, **10**, 948-952.
8. B. A. Pinaud, P. C. K. Vesborg and T. F. Jaramillo, *J. Phys. Chem. C*, 2012, **116**, 15918-15924.
9. Z. Li, W. Luo, M. Zhang, J. Feng and Z. Zou, *Energy Environ. Sci.*, 2013, **6**, 347-370.
10. P. Zhang, J. J. Zhang and J. L. Gong, *Chem. Soc. Rev.*, 2014, **43**, 4395-4422.
11. M. J. Liao, J. Y. Feng, W. J. Luo, Z. Q. Wang, J. Y. Zhang, Z. S. Li, T. Yu and Z. G. Zou, *Adv. Funct. Mater.*, 2012, **22**, 3066-3074.
12. G. J. Liu, J. Y. Shi, F. X. Zhang, Z. Chen, J. F. Han, C. M. Ding, S. S. Chen, Z. L. Wang, H. X. Han and C. Li, *Angew. Chem.-Int. Edit.*, 2014, **53**, 7295-7299.
13. C. Zhen, L. Z. Wang, G. Liu, G. Q. Lu and H. M. Cheng, *Chem. Commun.*, 2013, **49**, 3019-3021.
14. J. G. Hou, Z. Wang, C. Yang, H. J. Cheng, S. Q. Jiao and H. M. Zhu, *Energy Environ. Sci.*, 2013,

6, 3322-3330.
15. J. Cao, L. Ren, N. Li, C. W. Hu and M. H. Cao, *Chem.-Eur. J.*, 2013, **19**, 12619-12623.
16. M. Li, W. Luo, D. Cao, X. Zhao, Z. Li, T. Yu and Z. Zou, *Angew. Chem. Int. Ed.*, 2013, **52**, 11016-11020.
17. Y. Kado, C.-Y. Lee, K. Lee, J. Müller, M. Moll, E. Spiecker and P. Schmuki, *Chem. Commun.*, 2012, **48**, 8685-8687.
18. S. S. K. Ma, T. Hisatomi, K. Maeda, Y. Moriya and K. Domen, *J. Am. Chem. Soc.*, 2012, **134**, 19993-19996.
19. Y. B. Li, L. Zhang, A. Torres-Pardo, J. M. Gonzalez-Calbet, Y. H. Ma, P. Oleynikov, O. Terasaki, S. Asahina, M. Shima, D. Cha, L. Zhao, K. Takanabe, J. Kubota and K. Domen, *Nat. Commun.*, 2013, **4**, 2566.
20. J. Y. Feng, D. P. Cao, Z. Q. Wang, W. J. Luo, J. J. Wang, Z. S. Li and Z. G. Zou, *Chem.-Eur. J.*, 2014, **20**, 16384-16390.
21. S. Grigorescu, B. Bärhausen, L. Wang, A. Mazare, J. E. Yoo, R. Hahn and P. Schmuki, *Electrochem. Commun.*, 2015, **51**, 85-88.
22. A. B. Murphy, P. R. F. Barnes, L. K. Randeniya, I. C. Plumb, I. E. Grey, M. D. Horne and J. A. Glasscock, *Int. J. Hydrog. Energy*, 2006, **31**, 1999-2017.
23. M. Ritala, P. Kalsi, D. Riihela, K. Kukli, M. Leskela and J. Jokinen, *Chem. Mater.*, 1999, **11**, 1712-1718.
24. S. J. Henderson and A. L. Hector, *J. Solid State Chem.*, 2006, **179**, 3518-3524.
25. J. J. Wang, J. Y. Feng, L. Zhang, Z. S. Li and Z. G. Zou, *Phys. Chem. Chem. Phys.*, 2014, **16**, 15375-15380.
26. M. Harb, L. Cavallo and J.-M. Basset, *J. Phys. Chem. C*, 2014, **118**, 20784-20790.
27. M. Harb, P. Sautet, E. Nurlaela, P. Raybaud, L. Cavallo, K. Domen, J.-M. Basset and K. Takanabe, *Phys. Chem. Chem. Phys.*, 2014, **16**, 20548-20560.
28. J. Wang, T. Fang, L. Zhang, J. Feng, Z. Li and Z. Zou, *J. Catal.*, 2014, **309**, 291-299.
29. J. Wang, W. Luo, J. Feng, L. Zhang, Z. Li and Z. Zou, *Phys. Chem. Chem. Phys.*, 2013, **15**, 16054-16064.
30. E. Watanabe, H. Ushiyama and K. Yamashita, *Chem. Phys. Lett.*, 2013, **561**, 57-62.
31. G. Kresse and J. Furthmüller, *Comp. Mater. Sci.*, 1996, **6**, 15-50.
32. G. Kresse and J. Hafner, *Phys. Rev. B*, 1993, **47**, 558.
33. P. E. Blöchl, *Phys. Rev. B*, 1994, **50**, 17953.
34. J. P. Perdew, J. Chevary, S. Vosko, K. A. Jackson, M. R. Pederson, D. Singh and C. Fiolhais, *Phys. Rev. B*, 1992, **46**, 6671.
35. J. P. Perdew, K. Burke and M. Ernzerhof, *Phys. Rev. Lett.*, 1996, **77**, 3865-3868.
36. J. Heyd, G. E. Scuseria and M. Ernzerhof, *J. Chem. Phys.*, 2003, **118**, 8207-8215.
37. F. Bottin, F. Finocchi and C. Noguera, *Phys. Rev. B*, 2003, **68**, 035418.
38. N. E. Brese, M. O'Keeffe, P. Rauch and F. J. DiSalvo, *Acta Crystallogr. Sect. C: Cryst. Struct. Commun.*, 1991, **47**, 2291-2294.
39. C. Noguera, *J. Phys.: Condens. Matter*, 2000, **12**, R367.
40. C. M. Fang, E. Orhan, G. De Wijs, H. Hintzen, R. de Groot, R. Marchand and J.-Y. Saillard, *J. Mater. Chem.*, 2001, **11**, 1248-1252.
41. J. M. Morbec, I. Narkeviciute, T. F. Jaramillo and G. Galli, *Phys. Rev. B*, 2014, **90**, 155204.
42. J. Wang, A. Ma, Z. Li, J. Jiang, J. Feng and Z. Zou, *Phys. Chem. Chem. Phys.*, 2015, **17**,

8166-8171.
43. P. Tasker, *J. Phys. C: Solid State Phys.*, 1979, **12**, 4977-4984.
44. R. F. W. Bader, *Chem. Rev.*, 1991, **91**, 893-928.
45. D. Lu, M. Hara, T. Hisatomi, T. Takata and K. Domen, *J. Phys. Chem. C*, 2009, **113**, 17151-17155.

Table 1 The charge integrated on Cl and the adsorption energies (E_{ads}) of Cl on (100)+O_{N3}, $(010)_{T2}$+O_{N3} and $(001)_{T2}$+O_{N3} surfaces. The charge integrated on Cl is relative to the number of valence electrons of Cl (7).

Surfaces	Charge on Cl (electrons)	E_{ads} (eV)
(100)+O_{N3}	0.58	3.96
$(010)_{T2}$+O_{N3}	0.63	4.45
$(001)_{T2}$+O_{N3}	0.44	1.55

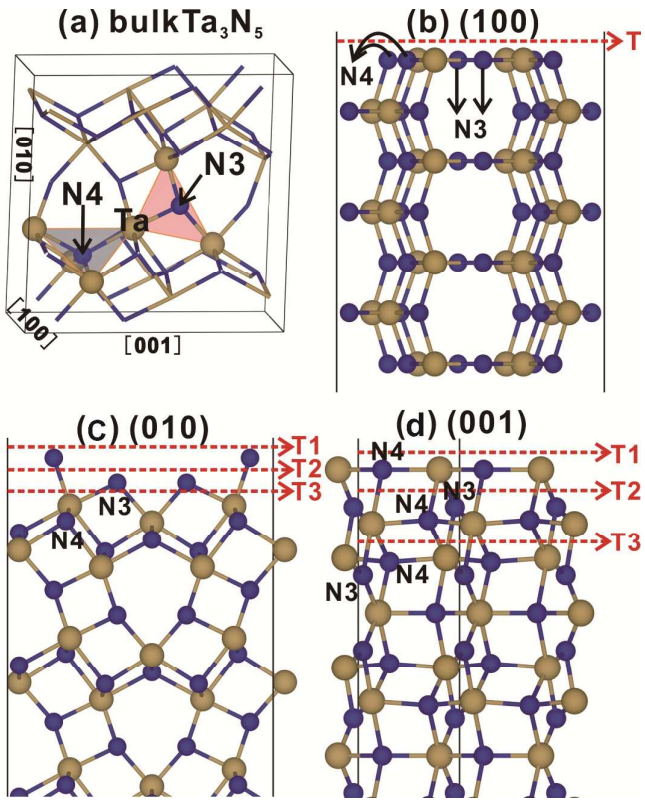

Fig. 1 Atomic structures of (a) the conventional cell of bulk Ta_3N_5, (b) (100), (c) (010) and (d) (001) surfaces of Ta_3N_5. In (b) to (c), possible terminations for each surface are labeled. For the visualization purpose, only one side of each slab is depicted, and the slab in (d) is extended by two times.

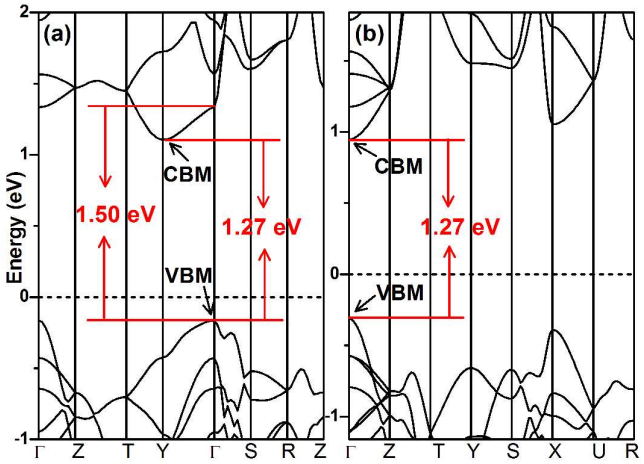

Fig. 2 Band structures calculated by the (a) primitive cell and (b) conventional cell of pure bulk Ta_3N_5.

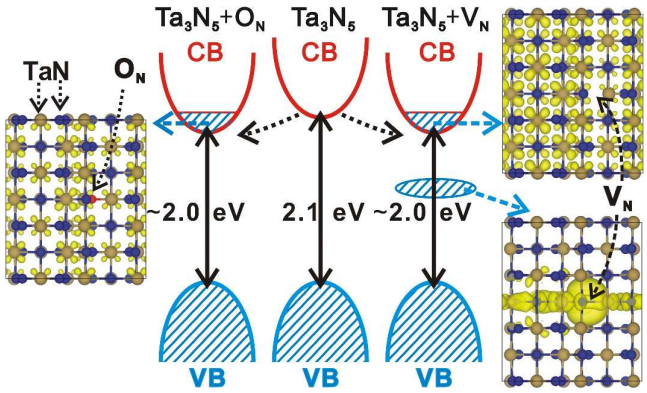

Fig. 3 Schematic diagram of the band structures of bulk Ta_3N_5, Ta_3N_5+O_N and Ta_3N_5+V_N (data derive from Ref. 42). The blue shaded area denotes the electron occupied states. The partial charge densities (in yellow) of the CBM and in-gap states for Ta_3N_5+O_N and Ta_3N_5+V_N are shown near the band structures.

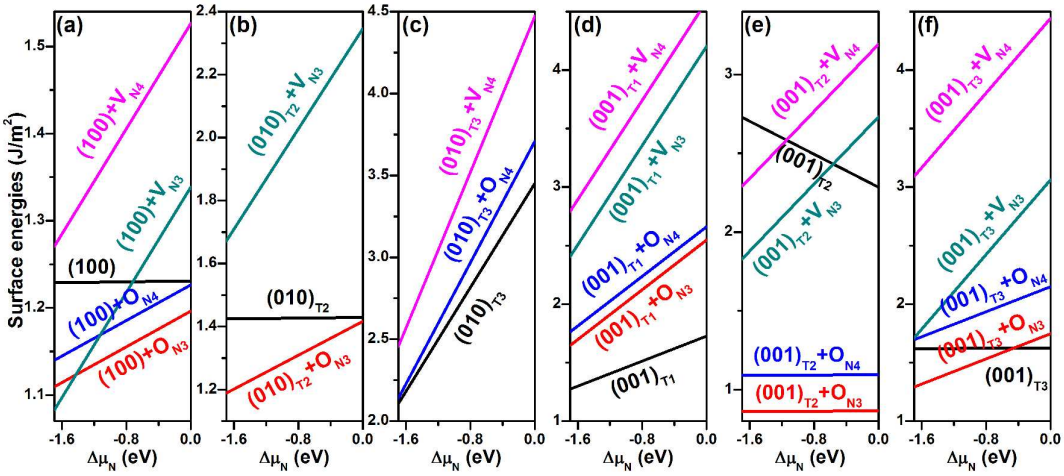

Fig. 4 Surface energies of Ta_3N_5 (a) (100), (b) $(010)_{T2}$, (c) $(010)_{T3}$, (d) $(001)_{T1}$, (e) $(001)_{T2}$ and (f) $(001)_{T3}$ surfaces with and without defects as a function of the chemical potential of N ($\Delta\mu_N$). The negative and zero values of $\Delta\mu_N$ correspond to N-poor and N-rich growth conditions, respectively.

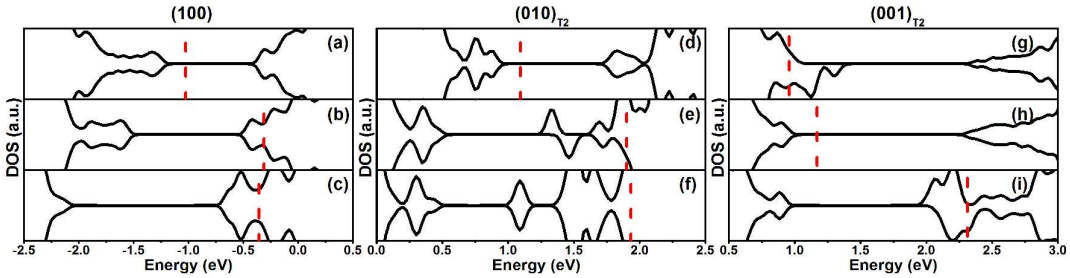

Fig. 5 DOS of Ta_3N_5 (a-c) (100), (d-f) $(010)_{T2}$ and (g-i) $(001)_{T3}$ surfaces with and without O_{N3} and V_{N3}. The DOS in (a-c) [the same for (d-f) and (g-i)] correspond to (100), (100)+O_{N3} and (100)+V_{N3}, respectively. The vertical red dash line in each case is the Fermi level. In (a-c) [the same for (d-f) and (g-i)], the horizontal axes of (b) and (c) are aligned with that of (a) by the electrostatic potentials.

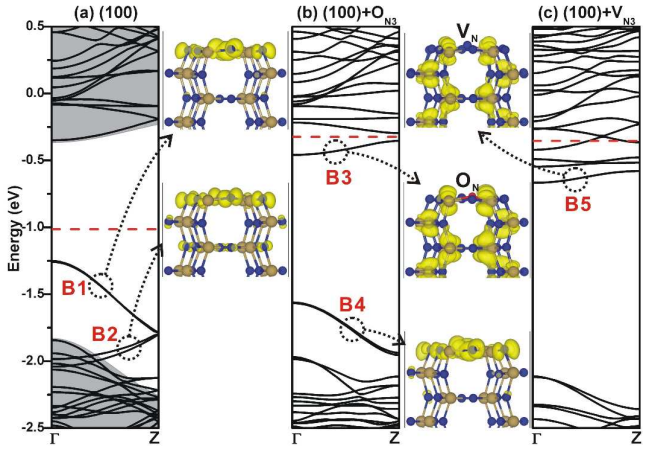

Fig. 6 Surface band structures of Ta_3N_5 (a) (100), (b) (100)+O_{N3} and (c) (100)+V_{N3}. The horizontal red dash line is the Fermi level. In (a), the shaded area is the projected band structure corresponded to the clean (100) surface. In each case, the partial charge densities (in yellow) of some labeled states are shown near the band structures (isosurface level = 0.001 electron per $Å^3$).

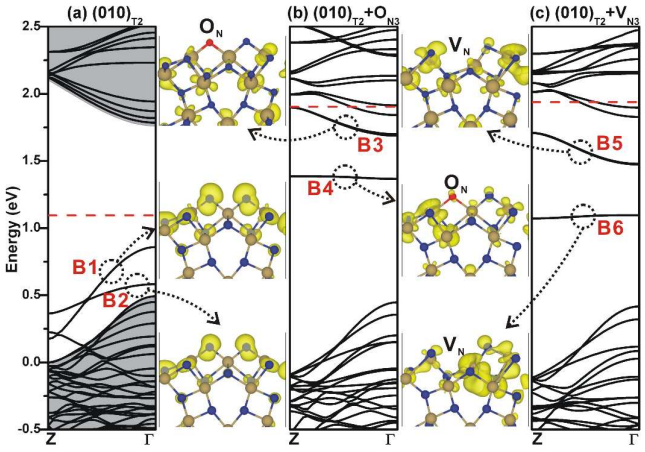

Fig. 7 The same as Fig. 6 but for Ta_3N_5 (a) $(010)_{T2}$, (b) $(010)_{T2}$+O_{N3} and (c) $(010)_{T2}$+V_{N3}.

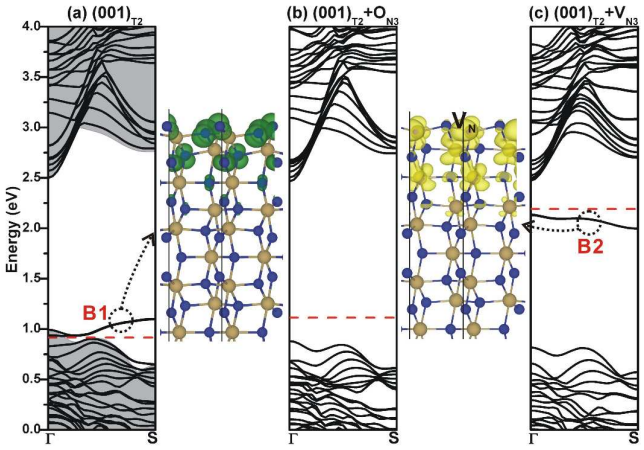

Fig. 8 The same as Fig. 6 but for Ta_3N_5 (a) $(001)_{T2}$, (b) $(001)_{T2}$+O_{N3} and (c) $(001)_{T2}$+V_{N3}. The green and yellow charge densities correspond to the holes and electrons occupied states, respectively.